Observations of interior whispering gallery modes in asymmetric optical resonators with rational caustics

Jie Gao[a)]
Optical Nanostructures Laboratory, Columbia University, New York, New York 10027, USA

Pascal Heider[b)]
Center of Mathematics Research, Bell Laboratories, Murray Hill, New Jersey 07974, USA

Charlton J. Chen, Xiaodong Yang, Chad A. Husko, and Chee Wei Wong
Optical Nanostructures Laboratory, Columbia University, New York, New York 10027, USA

(Received 16 July 2007; accepted 27 September 2007; published online 29 October 2007)

We propose asymmetric resonant cavities with rational caustics and experimentally demonstrate interior whispering gallery modes in monolithic silicon mesoscopic microcavities. These microcavities demonstrate unique robustness of cavity quality factor against roughness Rayleigh scattering. Distinct resonant families and directional radiation from interior whispering gallery modes are observed experimentally using angle-resolved tapered fiber measurements and near-field images, which can be used for microcavity laser and cavity quantum electrodynamics applications. © *2007 American Institute of Physics*. [DOI: 10.1063/1.2800308]

Photon confinement and processes in microcavities[1–3] are critical for a vast span of fundamental studies and applications, ranging from ultralow threshold microcavity lasers, nonlinear frequency generation,[4,5] dynamic filters, and memory for communications, to interactions of atoms with cavity modes in both strong and weak coupling regimes in cavity quantum electrodynamics (QED).[6,7] Characterized by the cavity quality factor (Q, photon lifetime) and modal volume (V, field intensity per photon), two-dimensional (2D) disklike resonant structures have achieved remarkable Q up to $\sim 10^8$ with $V \sim 450(\lambda/n)^3$.[2] A desirable characteristic of these planar whispering gallery mode resonators is that of directional emission, without significant Q spoiling from the loss of rotational symmetry.[8–11] Different approaches have been explored to show directional lasing from certain special cavity modes in far field distribution by deforming semiconductor or polymer circular microcavities into quadrupole shape,[8] stadium,[12] spiral shape, and line defect[13] with a critical and optimized deformation parameter. These asymmetric resonant cavities (ARCs) also have potential applications in the study of disorder and localization in mesoscopic systems as well as quantum chaos[14] in the diffusive limit. In this letter, we show our unique approach to design ARC with interior whispering gallery modes and characterize their directional radiation in monolithic silicon microcavities using angle-resolved tapered fiber coupling techniques and near-field images.

The ARCs we construct here possess whispering gallery modes spatially located deep inside the resonator.[15] These cavities have the special property that one can inscribe into the boundary a one-parametric family of p-periodic orbits of the associated billiard map. The shapes of such resonators are constructed numerically as a solution of a nonholonomic dynamical system.[15] Here we demonstrate a class of resonators with a family of four-periodic orbits. The involute of all these four-periodic orbits forms the rational caustic of the shape. In the surface of section (SOS) plot which represents the classical ray motion in phase space,[16] a rational caustic corresponds to an invariant curve consisting of periodic orbits. Under slight perturbation this curve breaks up and a near integrable region appears with the usual periodic orbits surrounded in phase space by elliptic islands, invariant curves, and chaotic regions. This region can be seen in the SOS of Fig. 1(a) which is called the interior whispering gallery (IWG) region. One would expect a family of quasimodes or resonances localized near the original rational caustic. Light will mainly escape at the location where the near integrable region resulting from the rational caustic is closest to the line of total internal reflection. Emission is expected to have strong directionality where half of the total radiation

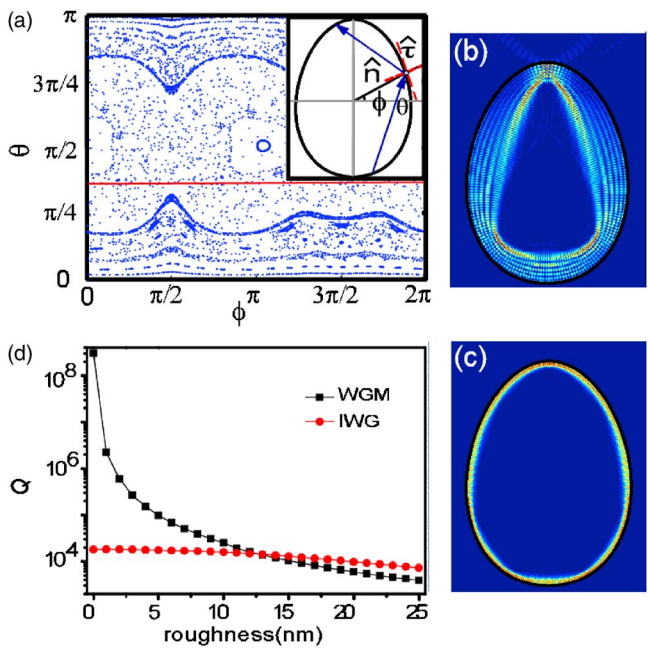

FIG. 1. (Color online) (a) Poincaré surface of section plot. Horizontal axis φ represents the intercept point of the ray and the cavity boundary, and vertical axis θ represents the incident angle between the ray and the tangent line of the boundary. The red solid line corresponds to the total internal reflection. (b) IWG mode supported near the rational caustic and (c) the fundamental WGM mode. (d) Numerical simulations of Q for WGMs (squares) and IWG modes (circles) vs cavity edge roughness.

a)Electronic mail: jg2499@columbia.edu
b)Electronic mail: pheider@research.bell-labs.com

comes from positions according to $\Phi=90°$, $\theta\sim45°$ or 135° in SOS map with lateral divergence angle of ~11° in the azimuthal direction.

Analogous to whispering gallery modes (WGMs) which are shown in Fig. 1(c) and has $Q\approx3.0\times10^8$, one can also find a family of IWG modes which are supported near the rational caustic and has $Q\approx1.8\times10^4$, as shown in Fig. 1(b). We calculate TM modes and Q factors by reducing the three-dimensional Maxwell equations to a 2D resonance problem and solve this with a boundary integral method.[17] The size and geometry of the ARC in the simulations are the same with the fabricated ARC. Our analysis also shows that these IWG modes have linear modal volumes $\sim10(\lambda/n)^3$ and nonlinear modal volumes $\sim50(\lambda/n)^3$.[5] In order to study the intrinsic loss mechanisms in the ARC, slight perturbations to the cavity shape are introduced to investigate numerically the effects of sidewall disorder roughness (in the actual fabrication) on Q for both the fundamental WGMs and IWG modes. The intrinsic loss mechanisms in microcavities include radiation loss, scattering loss, material absorption, and surface absorption.[18] For microdisks with current modal volumes, surface and material absorption-limited Q are typically on the order of 10^6.[18] Because experiments of the fabricated ARCs show that total Q are on the order of 10^3, surface and material absorption losses are negligible here. For WGMs, the radiation Q is theoretically $\sim10^8$ so that surface scattering will predominantly dominate the total loss. However, for IWG modes, the radiation Q is around 10^4 due to the intentionally constructed asymmetric shape for directional emission so that radiation is the major loss mechanism for ARC with small edge roughness. When the roughness is large enough, scattering loss will turn out to be comparable to radiation loss. Figure 1(d) shows an exponential drop of Q for the WGM with increased edge roughness, whereas Q for the IWG is only slightly affected by a perturbation larger than 15 nm. Even when the roughness is larger than 20 nm, we still get a less significant spoiling of Q by boundary imperfection for IWG modes than for WGMs because IWG modes are mostly concentrated along the rational caustic and away from the boundary.

Having designed this special class of ARC, we fabricate the resonators from silicon-on-insulator wafers consisting of a 200 nm thick Si layer on top of a 3 μm SiO_2 cladding layer with electron-beam lithography and inductively coupled-plasma reactive-ion etch. The SiO_2 layer is etched in buffered hydrofluoric acid to suspend the microdisklike structures.[19] An example scanning electron micrograph (SEM) of a microfabricated resonator is illustrated in Fig. 2(b), with an estimated line-edge roughness of 17 nm.

To characterize the silicon ARC, a tapered optical fiber setup such as described in Refs. 20 and 21 is used. By keeping an adiabatic taper profile, a SMF-28 fiber is pulled into a tapered fiber with ~1.1 μm waist diameter and negligible loss. The tapered fiber is then curved to provide coupling and contact with the edge of the ARC.[20] The radius of curvature of the curved tapered fiber is ~150 μm. Light from an amplified spontaneous emissions source, passing through an in-line fiber polarizer and a polarization controller, is evanescently coupled into cavity through tapered fiber. The imaging system consists of a 50× long working distance objective lens and an 8× telescope. Figure 2(a) shows the taper transmission spectra at different coupling positions [(1)–(4)] [as defined in Fig. 2(b)] for TM-like modes. Different coupling

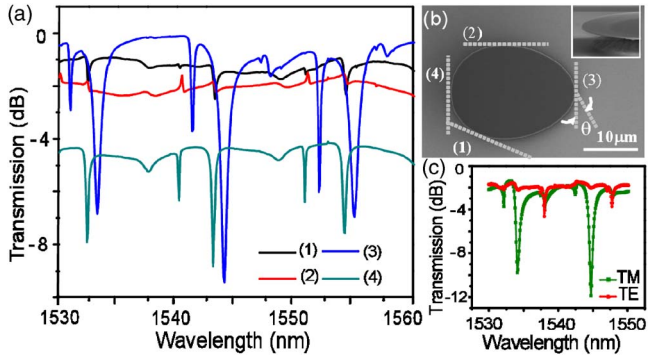

FIG. 2. (Color online) (a) Normalized transmission spectra when the taper touches the resonator side in tangential direction at different positions. (b) SEM of fabricated suspended silicon ARC on oxide pedestal. Dotted lines (--) show tapered fiber spatial probe positions [(1)–(4)]. (c) Transmission spectrum for TE-like and TM-like polarizations.

depths at each position reflect the asymmetric property of this resonator. Positions (3) and (4) show better coupling efficiency due to the strongest mode overlap in the evanescent field with the curved tapered fiber. At positions (1) and (2), the coupling to the resonant modes does not show strongly and asymmetric Fano lineshapes[22] also appear which we suspect are due to an interference pathway between a direct background (weak tapered fiber cavity) and indirect resonant (ARC) pathway. Figure 2(c) shows transmission for both TE-like and TM-like polarizations at position (3). TM-like mode is selected in measurement due to its stronger coupling and significantly reduced sensitivity to cavity edge roughness.[19]

We perform our tapered fiber coupling measurements along different coupling angles to study the radiation directionality. The transmission spectra in Fig. 3(a) show that two distinct mode families with free spectral range of ~11 nm are strongly supported in this ARC. To identify these families, we examined the coupling depth versus θ [the coupling

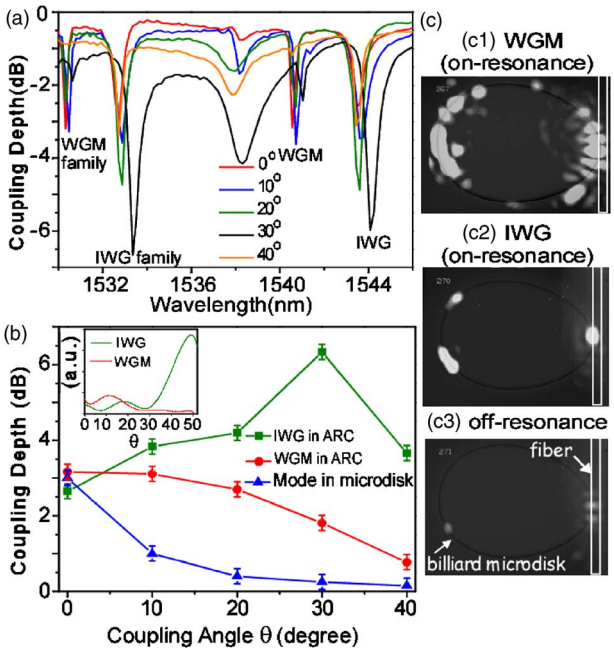

FIG. 3. (Color online) (a) Normalized transmission spectra when the taper is positioned along different coupling angles θ at position (3). (b) Experimental and numerical (inset) results for coupling depth vs θ. (c) Near-field images of IWG modes (c2) and WGMs (c1).

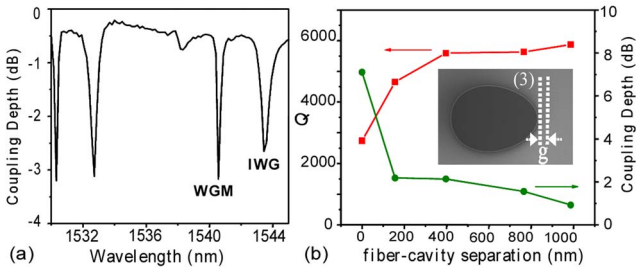

FIG. 4. (Color online) (a) Transmission spectrum when fiber-cavity separation $g=0$. (b) Coupling depth (circles) and Q factor (squares) as functions of g. Inset: experiment illustration for measuring the Q value.

angle between the resonator and the fiber as defined in Fig. 2(b)] at position (3). In Fig. 3(b), there exists a critical angle $\theta \sim 30°$ for the IWG modes where best coupling occurs. For the WGMs, no peaks appear and the coupling depth decreases continuously, which shows that the mode overlap between the WGMs and fiber mode decreases when the tapered fiber is far away from the tangent position. This gives a clear indication that we can distinguish IWG modes and WGMs from different coupling-angle dependences. The strongest coupling strength tells us that the cavity mode radiation is strongest in this direction, which matches consistently with our numerical predictions of directional emission. We also perform control measurements of WGMs in circular microdisk as a comparison. The coupling depth decreases exponentially as we expect, and the slight discrepancy between the WGMs in our ARC and WGMs in circular microdisk is due to the asymmetric shape of our resonator. Inset of Fig. 3(b) shows calculated mode overlaps, which are proportional to the coupling depths, between cavity modes and the fiber mode. We observe consistently the strongest mode overlap between the IWG modes and the fiber mode at $\theta \sim 45°$, which matches our experimental result. We attribute the offset between the measured and calculated peak positions primarily to the small deviation between our design and the actual shape, and uncertainties in the exact angular determination.

To investigate individual mode distribution in ARC, Fig. 3(c) shows the near-field images using a tunable laser and a ThermCAM Merlin near-infrared camera. When the wavelength is tuned on-resonance with the IWG mode, as shown in Fig. 3(c2), only three bright scattering regions which represent the directional emission of the ARC are observed. This corresponds directly to three regions of high intensity in the IWG mode shown in Fig. 1(b), and also agrees with three peaks within the IWG region in the SOS map in Fig. 1(a). For comparison Fig. 3(c1) shows WGM mode when tuned on-resonance, and scattering from the entire boundary can be observed. This confirms our simulation result that scattering loss of WGM modes due to edge roughness is dominated while IWG modes is not sensitive as WGM to Rayleigh scattering from edge roughness. As a reference, a near-infrared image with off-resonance condition is also illustrated in Fig. 3(c3), where only the fiber mode is observable.

To characterize the quality factor of IWG modes, feedback-controlled piezoelectric stages are used to control the lateral taper-cavity separation g, which is illustrated in the inset of Fig. 4(b). The transmission spectrum in Fig. 4(a) shows a loaded Q of 2800 for IWG mode at 1543.44 nm when $g=0$. Note that the WGM typically shows a larger Q of 8000 than IWG mode due to the increased leakage of IWG modes from directional emission. In Fig. 4(b), the loading effect diminishes as g increases and the estimated intrinsic cavity Q is ~6000 for IWG mode. The measured Q deviates from the numerical predictions due to increased surface scattering in the vertical direction (not captured in simulations).

In summary, we have constructed numerical methods to design remarkable asymmetric resonant cavities with high Q interior whispering gallery modes and observed experimentally the radiation directionality of these modes with Q value of ~6000 through angle-resolved tapered fiber coupling techniques. The Q values of these modes are not spoiled by slight edge boundary imperfection, which is an advantage for application and proves the usefulness of resonators with rational caustics together with the directionality. Our design and characterization of interior whispering gallery modes in silicon asymmetric resonant cavities open the door to engineer the asymmetric cavity shape and achieve its application in microcavity-based QED and lasing with directional emission in the future.

The authors acknowledge support by the Columbia Initiative in Nanophotonics, NSF ECS 0622069, the New York State Office of Science, Technology and Academic Research. P.H. is supported by a Feodor Lynen scholarship of the Humboldt-Foundation. X.Y. is supported by an Intel fellowship. We thank Y. Baryshnikov, K. Srinivasan, and O. J. Painter for helpful discussions and suggestions, and B. Lee and K. Bergman for near-infrared camera. J. Gao and P. Heider contribute equally to this work.

[1] *Optical Processes in Microcavities*, Advanced Series in Applied Physics Vol. No. 3, edited by R. K. Chang and A. J. Campillo (World Scientific, Singapore, 1996), Vol. 3, p. 389.
[2] *Optical Microcavities*, Advanced Series in Applied Physics Vol. No. 5, edited by K. J. Vahala (World Scientific, Singapore, 2005), Vol. 5, p. 415; K. J. Vahala, Nature (London) **424**, 839 (2003).
[3] S. Noda, M. Fujita, and T. Asano, Nat. Photonics **1**, 449 (2007).
[4] T. Carmon and K. Vahala, Nat. Phys. **3**, 430 (2007).
[5] X. Yang and C. W. Wong, Opt. Express **15**, 4763 (2007).
[6] T. Aoki, B. Dayan, E. Wilcut, W. P. Bowen, A. S. Parkins, T. J. Kippenberg, K. J. Vahala, and J. Kimble, Nature (London) **443**, 671 (2006).
[7] R. Bose, X. Yang, R. Chatterjee, J. Gao, and C. W. Wong, Appl. Phys. Lett. **90**, 111117 (2006).
[8] C. Gmachl, F. Capasso, E. E. Narimanov, J. U. Nockel, A. D. Stone, J. Faist, D. L. Sivco, and A. Y. Cho, Science **280**, 1556 (1998).
[9] A. F. J. Levi, R. E. Slusher, S. L. McCall, J. L. Glass, S. J. Pearton, and R. A. Logan, Appl. Phys. Lett. **62**, 561 (1993).
[10] H. G. L. Schwefel, N. B. Rex, H. E. Tureci, R. K. Chang, A. D. Stone, T. Ben-Messaoud, and J. Zyss, J. Opt. Soc. Am. B **21**, 923 (2004).
[11] J. Wiersig and M. Hentschel, Phys. Rev. A **73**, 031802(R) (2006).
[12] W. Fang, H. Cao, and G. S. Solomon, Appl. Phys. Lett. **90**, 081108 (2007).
[13] A. Tulek and Z. V. Vardeny, Appl. Phys. Lett. **90**, 161106 (2007).
[14] A. Kudrolli, V. Kidambi, and S. Sridhar, Phys. Rev. Lett. **75**, 822 (1995).
[15] Y. Baryshnikov, P. Heider, W. Parz, and V. Zharnitsky, Phys. Rev. Lett. **93**, 133902 (2004).
[16] L. Reichl, *The Transition to Chaos in Conservative Classical Systems: Quantum Manifestations* (Springer, New York, 1992), Chap. 2, p. 24.
[17] Jan Wiersig, J. Opt. A, Pure Appl. Opt. **5**, 53 (2003).
[18] M. Borselli, T. J. Johnson, and O. J. Painter, Opt. Express **13**, 1515 (2005).
[19] M. Borselli, K. Srinivasan, P. E. Barclay, and O. J. Painter, Appl. Phys. Lett. **85**, 3693 (2005).
[20] I.-K. Hwang, S.-K. Kim, J.-K. Yang, S.-H. Kim, S. H. Lee, and Y.-H. Lee, Appl. Phys. Lett. **87**, 131107 (2005).
[21] K. Srinivasan, P. E. Barclay, M. Borselli, and O. Painter, IEEE J. Sel. Areas Commun. **23**, 1321 (2005).
[22] X. Yang, C. Husko, C. W. Wong, M. Yu, and D.-L. Kwong, Appl. Phys. Lett. **91** 051113 (2007).